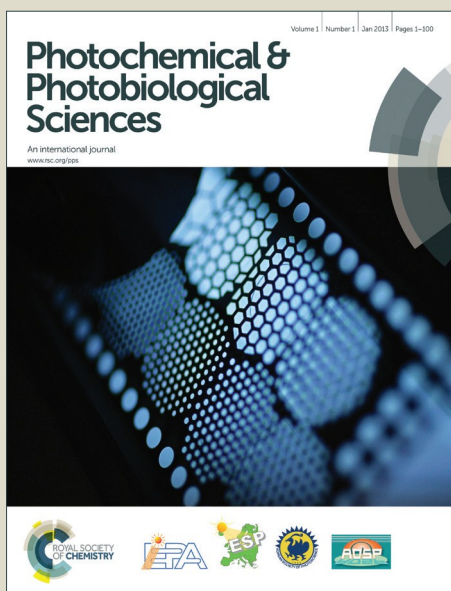


Photochemical & Photobiological Sciences

Accepted Manuscript



This is an *Accepted Manuscript*, which has been through the Royal Society of Chemistry peer review process and has been accepted for publication.

Accepted Manuscripts are published online shortly after acceptance, before technical editing, formatting and proof reading. Using this free service, authors can make their results available to the community, in citable form, before we publish the edited article. We will replace this *Accepted Manuscript* with the edited and formatted *Advance Article* as soon as it is available.

You can find more information about *Accepted Manuscripts* in the [Information for Authors](#).

Please note that technical editing may introduce minor changes to the text and/or graphics, which may alter content. The journal's standard [Terms & Conditions](#) and the [Ethical guidelines](#) still apply. In no event shall the Royal Society of Chemistry be held responsible for any errors or omissions in this *Accepted Manuscript* or any consequences arising from the use of any information it contains.

Photo-Active Float for Field Water Disinfection

Shwetharani R and R Geetha Balakrishna*

Centre for Nano and Material Sciences, Jain University, Jain Global Campus, Bangalore -562112, India

***Corresponding author's full mailing address:**

Dr. R. Geetha Balakrishna,

Director & Professor,

Centre for Nano and Material Sciences,

Jain University,

Jakkasandra post, Kanakapura Taluk,

Bangalore Rural district- 562112

Phone: + 91 8027577212

Fax: + 91 8027577211

cnms.jainuniversity.ac.in

*e-mail: br.geetha@jainuniversity.ac.in

Abstract:

The present study investigates the antibacterial activity of a photoactive float fabricated with visible light active N-F-TiO₂ for disinfection of field water widely contaminated with gram positive and gram negative bacteria like, *Salmonella typhimurium* (gram negative), *Escherichia coli* (gram negative), *Staphylococcus aureus* (gram-positive), *Bacillus species* (gram-positive), and *Pseudomonas species* (gram negative). The antibacterial activity can be attributed to the unique property of the photocatalyst, which releases reactive oxygen species in aqueous solution, under the illumination of sun light. N-F-TiO₂ nanoparticles efficiently photocatalysis the destruction of all the bacteria present in the contaminated water, giving a clean water. The inactivation of bacteria is confirmed by standard plate count method, MDA, RNA and DNA analysis. The purity of water was further validated by SPC indicating nil counts of bacteria after its two days of storing and testing. The photocatalysts were characterized by XRD, BET measurement, SEM, EDX, UV–Vis and PL analysis.

Key words: *TiO₂, Bacterial inactivation, NF-TiO₂, Semiconductor, Field water.*

1. Introduction:

Lack of access to safe drinking water is one of the pervasive problems affecting the people around the world causing water scarcity even in the regions historically considered as abundant in water resources ¹. Dominance of pathogenic microorganisms in water is perhaps the most important human health problem related to the use of unsafe drinking water. Waterborne infectious agents responsible for these diseases include a variety of bacteria, fungi and viruses, which causes intestinal parasitic infections and diarrheal diseases caused by waterborne bacteria and enteric viruses have become a leading cause of malnutrition owing to poor digestion of the food eaten by people sickened by water ². The alternative antibacterial techniques that are available includes the treatment of volatile fatty acid (VFA) ³, ultraviolet light irradiation, ozone treatment, low frequency ultrasonic irradiation, reverse osmosis processes, combinations of different hurdles, including moderately high temperatures (<60 °C), antimicrobial compounds, and pulsed electric field (PEF) ⁴ or combinations of levulinic acid and sodium dodecyl sulfate ⁵ have their disadvantages and advantages. An economical disinfection process, which utilizes renewable sunlight and without usage of nonrenewable source of energy is worthwhile to investigate. Nanoscale inorganic metal oxides are being increasingly used for antibacterial applications. The unique properties of nanoparticles, predominantly their small size and high surface-to-volume ratio, allow this technology to exceed barriers and gain access to **biological** molecules and system ⁶. For the past twenty years, the novel microbiocidal activities of TiO₂ through a photocatalytic reaction over *Escherichia coli* ⁷, *Penicillium expansum* ⁸, *Pseudomonas aeruginosa* ⁹, *Enterobacter cloacae* ¹⁰, *Staphylococcus aureus* ¹¹, and virus and cancer cells ¹² have been reported. TiO₂ is presumed to be toxic to both gram-negative and gram-

positive bacteria¹³. Most of the researchers have worked selectively with one or more bacteria without advancing much to study the complete disinfection of field water with a number of unknown bacteria. The present paper reports the whole procedure from collection and identification of the bacteria in field water to complete disinfection to clean water and its validation. TiO₂ absorbs ultraviolet light preventing its practical efficiency for solar **applications**¹⁴⁻¹⁶. However, recently several modifications have been made to extend the light absorption capability of TiO₂ into visible light region by coupling with a narrow band gap semiconductor^{17, 18}, doping with transition metals (Fe, Co, Ag, Cr and Mo)¹⁹, codoping with two or more foreign ions, surface sensitization by organic dyes or metal complexes, surface fluorination, addition of a sacrificial agent (SA), different preparation techniques²⁰ and noble metal deposition which induces a substantial influence in modifying the electronic band structure and construction of favorable surface structure resulting in higher visible light absorption²¹⁻²³¹⁹,²⁴. Introduction of anionic dopants, especially nitrogen, to TiO₂ makes it possible to achieve band gap narrowing²⁵. Doping of two types of non metal atoms such as C and N atoms, S and N atoms, B and N atoms, and F and N atoms **show** more efficiency in contrast to single non metal dopant²⁶. It is well reported N and F codoping changes the electronic structures of the TiO₂ to significantly **lower bandgap** energy, which induces the absorption of visible light²⁶. **Nitrogen (N) doping is particularly favored because a) it forms N-induced mid band (N 2p) level, slightly above the (O 2p) valence band b) creates surface oxygen vacancies**²⁷. Fluorine (F) doping generates several beneficial effects such as creation of surface oxygen vacancies **and** Ti³⁺ ions, **reduced** radiative recombination of photogenerated excitons, favors the generation of more •OH radicals, **suppression of** the crystallization of rutile and brookite phases, and **enhanced** surface acidity for adsorption of agents²⁸. The present study utilizes the enhanced properties of

N-F-TiO₂ to deactivate multiple bacteria in field water using sunlight. Since the powder form of photocatalyst has a disadvantage of separation, a float **has been** developed by immobilizing the catalyst on a conducting substrate **such that it could float** on contaminated water to effectively deactivate the bacteria.

2. Experimental

2.1. Materials:

Titanium tetra chloride (99.5% loba Chemie), titanium tetra fluoride (97%), ethanol, ammonia (95%), urea (99%) and other chemicals namely sulphuric acid (98%, 36 N), ammonium hydroxide (30%), brain heart infusion agar (BHI), sodium chloride and sodium hydroxide (97%) **used** were of Merck brand.

2.2. Synthesis of Photocatalyst:

Preparation of TiO₂ was carried out as reported elsewhere²⁹. The N-F-doped TiO₂ was prepared by hydrothermal method. 10 ml titanium isopropoxide was added to 50 ml of ethanol with constant stirring for 20 min. Mixture of HNO₃, H₂O **and** ethanol (1:1:50) was added drop wise into the above solution and stirred until a uniform, transparent light yellow gel turned up. Saturated urea was chosen as nitrogen source and ammonium fluoride as fluoride source. Saturated urea **and** ammonium fluoride **were mixed** with the **above** solution and the pH was adjusted to ≤ 2.5 . **The** mixture had reacted for 8 hours at 180 °C in **a hydrothermal reactor** lined with teflon. The products were **then** cleaned by ultrapure water and absolute ethyl alcohol. After being dried at 80 °C in the oven and calcined for 1 hour at 500 °C in the muffle furnace, **a photo-active float was prepared from it as reported by Laveena et al²⁹.**

2.3. Characterization:

The prepared TiO₂ and N-F-doped TiO₂ samples were characterized by X-ray diffraction (XRD) patterns recorded by a Shimadzu X-ray diffractometer with Cu K α radiation at a scan rate of 1°/minute to study the crystal structure and crystallinity of TiO₂. The average size of particle was calculated based on XRD peak broadening using Scherrer's equation³⁰, where particle size = $K\lambda/\beta \cos\theta$, β = broadening of diffraction line measured at half maximum intensity; λ = wavelength of X-ray radiation; θ = Bragg angle and $K = 1$ for spherical particles. Energy dispersive X-ray (EDX) analysis was used in conjunction with scanning electron microscope (SEM; Quanta 200 FEI) to detect the elementary levels in powder samples. The absorption spectra were recorded by Shimadzu 1800 PC UV–visible spectrophotometer for micromolar suspensions of the catalysts, prepared by ball milling to avoid reflection of light, to a maximum extent. Photoluminescence (PL) experiments were performed on a Shimadzu RF 5301 PC spectrofluorometer.

2.4. Photocatalytic evaluation:

Field water (collected from Gabbadi lake, Bangalore, India) contaminated with *Salmonella typhimurium*, *Escherichia coli*, *Staphylococcus aureus*, *Bacillus cereus*, *shigella sp.*, and *Pseudomonas sp* was taken for the photocatalytic disinfection experiment. The identification of bacteria was confirmed by a spread method (a small volume of a bacterial suspension is distributed evenly over the surface of an agar plate using a smooth sterilized spreader) culturing on specific media's like SS (salmonella-shigella agar) agar plate, Eosin methylene blue (EMB) agar; Levine plate, Mannitol salt agar plate, Bacillus cereus agar plate and Pseudomonas fluorescein agar plate. However, presence of some very rare bacteria cannot be ruled out, which we couldn't identify. 0.6 g of photocatalyst has been coated on a weighed glued plastic sphere, which could float on a liter of contaminated **field** water which is incessantly stirred at a speed of

500 rpm at a depth of 8 cm in a 2 L beaker with an exposure area of 177 cm². **Photocatalytic** experiments were tested at various conditions, without light (dark), with light and in the absence of catalyst (control). **Photo** reactions was carried out on bright sunny days in the month of March between around 11 AM to 2.00 PM at Bangalore city (13⁰⁰00.57'N and 77⁰⁰34.15'E), which is about 1800 km from New Delhi, the capital of India. The average solar intensity was 998.8 W/m² and no steps were taken to maintain the intensity of sunlight during the reaction. The reaction **mixtures were** incessantly stirred **on** a magnetic stirrer in atmospheric oxygen during **photoreactions**. The samples were collected at every 15 min intervals like 0, 15, 30, 45, 60 and 90 min for analysis. The illuminated bacterial solutions were examined for the viable number of bacteria by standard plate count method, with triplicate testing, giving fairly good reproducibility. The samples **for the same** were serially diluted (1ml *10⁻⁴ dilution) and was plated on BHI agar and incubated at 37 °C for 24 h. Then the colonies were counted to determine the number of viable cells. Formation of malondialdehyde (MDA) in 1ml of the analyzed bacterial sample was used as an indicator to measure lipid peroxidation, to estimate the membrane damage³¹. The released RNA was determined by reaction with orcinol using RNA from baker's yeast as a standard and the absorbance was measured at 665 nm³². The DNA was estimated by reaction with diphenylamine using DNA from **salmon milt** as a standard and absorbance was measured at 595 nm. The protein concentration was measured by Lowry et al method with bovine serum albumin as a standard at a particular value of $\lambda_{\max} = 753 \text{ nm}$ ³³. The experimental values obtained are plotted as smooth curves using the spline curve in origin software.

3. Results and Discussion

The crystal structure of TiO₂/ NFTiO₂ synthesized by sol-gel/ hydrothermal method was analyzed by **the obtained** XRD patterns. Figure 1 shows the diffractograms recorded for TiO₂ and NFTiO₂. The diffraction peaks of as-prepared TiO₂ could be indexed to the anatase TiO₂ phase, representing that anatase TiO₂. Both the d-spacing and the intensities match with the corresponding pattern reported by JCPDS data of 100% anatase TiO₂ phase³⁰. The mean crystallite size of the TiO₂ nanoparticle was 15 nm. The crystal planes of anatase peaks (101) (211) and (004) were selected to determine the lattice parameters, $a = 3.7675 \text{ \AA}$ and $c = 9.4686 \text{ \AA}$. The cell volume was found to be 136.66 \AA^3 . The XRD patterns of NFTiO₂ showed similar peaks **but with a scanty change in lattice parameters ($a = 3.7332 \text{ \AA}$, $c = 9.4787 \text{ \AA}$), increase in crystallite size (to 16.91 nm) and cell volume (138.78 \AA^3)**. Figure 2 depicts the UV-visible absorption spectra of the synthesized photocatalysts. The absorption band of TiO₂ is observed **to be** at 392 nm with a band gap of 3.1 eV. Doping of TiO₂ with nitrogen and fluorine shows significant shift of absorption band towards visible region, consequently **decreasing** the band gap to 2.9 eV, because **of** the electron **transitions** between 2p states of nitrogen and conduction band of TiO₂. **This resulting** in lower energy absorption or red shift of the doped sample. Fig 3 illustrates the X-ray photoelectron spectrum of NFTiO₂ nanoparticle. Fig 3a depicts the wide spectrum of NFTiO₂ indicating the presence of Ti, O, N and F elements in the doped photocatalyst and a small peak 284.9 eV was attributed to carbon from the instrument. The Ti 2p core level spectrum contains Ti 2p_{1/2} and Ti 2p_{3/2} spin orbital splitting photoelectrons located at binding energies 458.5 and 464.2 eV as shown in Fig 3b, which are in agreement with the literature values. Fig 3c describes the O 1s core level spectra of catalyst. The O 1s peak was deconvoluted into three contributions at 531.6 eV, 532.4 eV, and 533.4 eV which corresponds to

Ti–O, O–Ti–N, and surface OH groups, respectively³⁴. The peaks in the range 394–398 eV were attributed to N 1s³⁵ and the peak at 398 eV corresponds to N–Ti–N bond³⁶. **Nitrogen** replaces oxygen atoms substantiating the effective doping of nitrogen into TiO₂ crystal lattice. **Binding** energies at 684 and 686 eV are attributed to F 1s core level³⁷ and the doping of F reduces the electron-hole pair recombination through charge compensation between F[–] and Ti⁴⁺, thus **creating** oxygen vacancies, which **could act** as traps for charge carriers **avoiding recombination**. **The charge carriers could later be detrapped from the surface states for oxidation reaction, thus enhancing** the efficiency of the photocatalyst as shown in Fig 3d. Fig 4a illustrates the surface morphology of TiO₂ nanoparticles, showing irregular shaped agglomerated particles with an average size of ~ 30 nm and the elemental composition of the TiO₂ as analyzed by EDX (Fig 4b) shows the presence of Ti and O element. Figure 5a demonstrates the SEM image of the prepared NFTiO₂ with lopsided particles having average size of 87 nm and the EDX analysis confirms the presence of N, F, Ti and O element indicating the absence of other impurities as shown in 5b respectively. NFTiO₂ with smaller particle size exhibit high antimicrobial activity because of both penetration and cell membrane **oxidation**. Specific surface area increases with decrease in particle size and the increase in surface area determine the potential number of reactive groups on the particle surface, on which bacteria will adsorb and cell membrane destruction takes place. Hence, smaller particles with larger surface to volume ratios have greater antibacterial activity³⁸. Fig 6 shows the photoluminescence spectra of TiO₂ and N–F–TiO₂, which is useful to understand the behavior of light-generated electrons and holes during photocatalysis in addition gives information about surface/ subsurface oxygen vacancies, lattice defects. It is known that the photoluminescence emissions on semiconductor materials are from the radiative recombination of photo-generated electrons and holes after being

activated by light. The photo excited electrons from the conduction band will return back to the valence band, with a release of energy as photoluminescence radiation. Lower fluorescence emission intensity implies delay in electron–hole recombination rate and high availability of the excitons for the photocatalytic reaction¹⁹. The graph shows decrease in emission for NFTiO₂ nanoparticles in comparison to TiO₂, indicating reduced recombination of e^-/h^+ in doped TiO₂. Titanium dioxide shows a broad and featureless emission peak at around 442 nm due to the radiative recombination of self trapped excitons. The NFTiO₂ shows peaks at 462, 431, 410 and 389 nm corresponding to the surface defects like oxygen vacancies, mid bands, which acts as traps for the charge carriers, thereby causing a delay in recombination. The delayed recombination makes the excitons (e^-/h^+) available for photocatalysis in NFTiO₂ to a great extent compared to TiO₂, thereby increases production of ROS leading to efficient disinfection. Fig 7 depicts the presence of five bacteria in field water. ***Bacillus cereus* in field water was confirmed by Bacillus cereus agar plate, salmonella and shigella sp., by SS agar plate, Escherichia coli by EMB agar; Levine plate, Pseudomonas sp by Pseudomonas fluorescein agar plate and Staphylococcus aureus by Mannitol salt agar plate.**

The efficiency of NFTiO₂ as antibacterial agent is demonstrated by its growth inhibition capacity against various bacterial forms randomly distributed in the contaminated field water. NFTiO₂ being a semiconductor with a band gap of 2.9 eV when exposed to solar light **causes the** electrons in the valence band **to be** excited to the conduction band leaving behind holes (h^+). The electrons which do not undergo recombination can reduce molecular O₂ to produce superoxide ions (O₂^{•-}), which further disproportionate to form more HO[•] radicals³⁹ and holes in the valence band to react with H₂O or hydroxide ions adsorbed on the surface to produce reactive hydroxyl radicals (OH[•]). Hence, the photocatalyst mediated reactions cause the generation of a number of

reactive oxygen species (ROS) and hydroxyl radicals. The reactive oxygen species (ROS) were able to oxidize the cell membrane lipids, causing a phenomenon called lipid peroxidation followed by destruction of cell membrane. Fig 8 depicts the plot of survival fraction (N/N_0) obtained from SPC method, where N is the number of colonies obtained after an illumination time period t and N_0 is the number of colonies obtained before any **absorption** of light. The above tests were conducted in triplicate giving fairly good reproducibility. The graph illustrates 90 % of inactivation with in 120 min in presence of nanostructured N-F-TiO₂ photocatalyst and 70 % **disinfection with TiO₂ nanoparticles, in the presence of sun light**. The enhanced efficiency of **the** doped photocatalyst is attributed to **its** band gap narrowing by formation of N-induced mid-band (N-2p) level slightly above the valence band (O-2p), consequently shifting the absorption wavelength to visible region, which directly influences OH radical generation and hence cell destruction. As observed in the plots sunlight source alone (control) causes inactivation to a small extent and there is no inactivation in the absence of light (dark). At first oxidative damage takes place on cell wall, where photocatalyst makes first contact with intact cell ⁴⁰. At this stage when only cell wall is damaged loss of viability is less, as the cells tend to remain in VBNC (viable but non culturable) state and count of colonies obtained on culturing fails to indicate the viable bacteria which are still pathogenic ^{41, 42}. It is important to completely destroy the pathogens and other analytical tools as mentioned below were helpful to validate the complete destruction of pathogens. Since the generated ROS interacts with the cell wall and its intracellular components like peptidoglycan, amino acids, and lipids, they give way for estimation. MDA is a lipid peroxidation product produced when ROS reacts with fatty acid on the cell membrane and forms lipid free radical, subsequently lipid peroxy radical, lipid hydroperoxide and finally malondialdehyde ⁴³. In addition MDA is an unstable and most

abundant aldehyde form produced from bacterial lipid membrane peroxidation and under photocatalytic reactions it undergoes further metabolic transformations. MDA has two aldehyde groups and the degradation products are estimated to be ring cleavage products, such as semialdehyde, malonate, monoaldehyde (formaldehyde, acetaldehyde), mono-ketons (acetone) and carboxylic acids (formic and/or acetic acid) or complete mineralization products such as CO_2 and H_2O ⁴⁴. Hence, the MDA values in each peroxidation lipidic test are the net result of its production and **its** photocatalytic degradation in oxidative condition. Thus, finally the plots represent the exceeded rate of MDA production over the rate of MDA destruction. The concentration of MDA in the treated sample confirms the peroxidation of cell wall components as shown in the Fig 9. The graph shows that MDA formation increases with time indicating the enhanced cell membrane damage with time. Final MDA concentration obtained on treatment with the NFTiO_2 photocatalyst was 22.2 nmol/mL, which was 1.8 and 3.8 times higher than TiO_2 and control respectively. SPC plots were exponential while the other plots appear linear. This is because the bacteria losses its culturing ability with in very short interval of light irradiation and hence most of the bacteria reaches VBNC state within 30 min of irradiation as shown in the exponential plots of SPC. The plots depicting the release of intra cellular components i.e. RNA, **DNA and protein were linear because the release was** gradual and proportional to irradiation time. Plots indicate that complete damage and death of bacteria required more time of irradiation. The plots indicate the release **of** DNA (Fig 10), RNA (Fig 11) and protein (Fig 12) on cell destruction by NFTiO_2 reaching 32.1 $\mu\text{g/mL}$, 1100 $\mu\text{g/mL}$ and 300.0 mg/L after 160 min of irradiation, clearly indicating the enhanced disinfection of water where in microorganisms are not only inactive but destroyed releasing the intracellular components. The so obtained water was further stored and tested for decontamination after two days by SPC, which depicted nil

counts of bacteria. Therefore it is reasonable to assume that the membrane is completely damaged by reactive oxygen species such as superoxide ($O_2^{\cdot-}$) or hydroxyl radicals (OH^{\cdot}) which are known to be produced from nanostructured photocatalyst^{45, 46}. As indicated in the SPC plot 90 % inactivation is observed at 120 min of light irradiation. Contrarily the release of intracellular components such as lipid, proteins, RNA and DNA continued beyond 120 min up to 160 min clearly **suggests** the existence of VBNC bacteria beyond 120 min. The present study signifies a 90 % disinfection of wide array of bacteria (both gram negative and gram positive) in field water using reusable photoactive float. Complete disinfection is not observed probably, due to the presence of other unidentified bacteria and the analytical estimation tools evident that SPC method is not proficient to detect VBNC bacteria and indicates that other investigative approaches are necessary. As per the guidelines of bacteriological standards of the USPH (United States public health drinking water standards) and ISI (Indian standard institution), the permissible **limit of** most probable number of pathogen existence is limited to 10 CFU/100 mL⁴⁷. Although the present work reports 10 CFU/ mL, which is slightly more, but still finds significance for **providing** an economical path to disinfect field water.

4. Conclusion:

Photocatalysis has proven to be an effective method for disinfection of field water contaminated with wide array of bacteria and the study also signifies the importance of other investigative approach along with SPC to validate the complete disinfection of water. N and F codoping effectively shifts the TiO_2 band gap energy to the visible region making it available for photocatalysis reaction in sunlight and hence generates large quantity of ROS compared to TiO_2 . ROS attacks the cell membrane, peroxidizes the lipid layer with the release of proteins, RNA and DNA followed by disintegration of cell. Other analytical techniques found that the damage in

cell structure and leakage of cell membrane constituents **take** much more time than VBNC state where SPC fails to detect the same. The study also signifies the utilization of photoactive float, which makes the process economical by avoiding separation of the catalyst and adding the advantage of recyclability.

5. Acknowledgement

The authors greatly acknowledge DST, New Delhi and Jain University for the financial support.

6. References

1. J. H. Castillo, A. Bueno, M. A. Pelaez, J. L. Sanchez-Salas, D. D. Dionysiou and E. R. Bandala, *International Journal of Chemical Reactor Engineering*, 2013, **11**.
2. A. A. Lima, S. R. Moore, M. S. Barboza Jr, A. M. Soares, M. A. Schlepner, R. D. Newman, C. L. Sears J. P. Nataro, D. P. Fedorko, T. Wuhib, J. B. Schorling and R. L. Guerrant, *The Journal of Infectious Diseases*, 2000, **181**, 1643–1651.
3. D.P. Kunte, T.Y. Yeole, S.A. Chiplonkar and D.R. Ranade, *Journal of Applied Microbiology*, 1997, **84**, 138–142.
4. M. Walkling-Ribeiro, F. Noci, D. A. Cronin, J. G. Lyng and D. J. Morgan, *Journal of Applied Microbiology*, 2009, **106**, 241-248.
5. P. Z. Tong Zhao and Michael P. Doyle, *Journal of Food Protection*, 2009, **72**, 928–936.
6. S. S. Sophee , R. G. S. V. Prasad, J. V. Srinivas, R. S. L. Aparna, and A. R. Phani, *Journal of Green Science and Technology*, 2012, **1**, 1-7.
7. Silvia Bonetta, Sara Bonetta, Francesca Motta, Alberto Strini and Elisabetta Carraro, *AMB Express* 2013, **3**, 1-8.

8. C. Maneerat and Y. Hayata, *International journal of food microbiology*, 2006, **107**, 99-103.
9. P. Amezaga-Madrid , G.V. Nevarez-Moorillon , E. Orrantia-Borunda ,M. Miki-Yoshida, *FEMS Microbiology Letters* 2002, **211**, 183-188.
10. J. A. Ibáñez, M. I. Litter and R. A. Pizarro, *Journal of Photochemistry and Photobiology A: Chemistry*, 2003, **157**, 81-85.
11. T. Asahara, H. Kosek, T. Tsurumoto, K. Shiraishi, H. Shindo, K. Baba and N. Terasaki, *Jpn. J. Infect. Dis.*, 2009, **62**, 378-380.
12. S. Sinha, T. Murugesan, K. Maiti, J. R. Gayen, B. Pal, M. Pal and B. P. Saha, *Fitoterapia*, 2001, **72**, 550-552.
13. L. K. Adams, D. Y. Lyon and P. J. Alvarez, *Water research*, 2006, **40**, 3527-3532.
14. S. Cao, B. Liu, L. Fan, Z. Yue, B. Liu and B. Cao, *Applied Surface Science*, 2014, **309**, 119-127.
15. K.U. Minchitha, R. Geetha Balakrishna, *Materials Chemistry and Physics*, 2012, **136**, 720-728.
16. L. P. D'Souza, V. Amoli, H. R. Chandan, A. K. Sinha, R. Krishna Pai and G. R. Balakrishna, *Solar Energy*, 2015, **116**, 25-36.
17. T C McGill and D A Collins, *Semicond. Sci. Techno*, 1993, **8**, 1-5.
18. W. H. Maksym, V. Kovalenko, Elena V. Shevchenko, Jong-Soo Lee, and A. P. A. Harald Schwinghammer, and Dmitri V. Talapin, *J. AM. CHEM. SOC.* , 2007, **129**, 11354-11355.
19. R. Shwetharani, C. A. N. Fernando and G. R. Balakrishna, *RSC Adv.*, 2015, **5**, 39122-39130.

20. Z. Peining, W. Yongzhi, M. V. Reddy, A. Sreekumaran Nair, P. Shengjie, N. Sharma, V. K. Peterson, B. V. R. Chowdaric and S. Ramakrishna, *RSC Advances*, 2012, **2**, 5123–5126.
21. M. V. Reddy, S. Adams, G. T. J. Liang, I. F. Mingze, H. Van Tu An and B. V. R. Chowdari, *Solid State Ionics*, 2014, **262**, 120-123.
22. C. T. Cherian, M. V. Reddy, T. Magdaleno, C.-H. Sow, K. V. Ramanujachary, G. V. S. Rao and B. V. R. Chowdari, *CrystEngComm*, 2012, **14**, 978-986.
23. M. V. Reddy, N. Sharma, S. Adams, R. P. Rao, V. K. Peterson and B. V. R. Chowdari, *RSC Adv.*, 2015, **5**, 29535-29544.
24. S. G. Kumar and L. G. Devi, *The journal of physical chemistry. A*, 2011, **115**, 13211-13241.
25. H. Choi, M. G. Antoniou, M. Pelaez, A. A. De la Cruz , J. A. Shoemaker, D. D. Dionysiou, *Environmental Science & Technology*, 2007, **41**, 7530-7535.
26. Y. Wu, M. Xing, B. Tian, J. Zhang and F. Chen, *Chemical Engineering Journal*, 2010, **162**, 710-717.
27. R. Asahi, T. Morikawa, T. Ohwaki, K. Aoki and Y. Taga, *Science*, 2001, **293**, 269-271.
28. Y. Lv, Z. Fu, B. Yang, J. Xu, M. Wu, C. Zhu and Y. Zhao, *Materials Research Bulletin*, 2011, **46**, 361-365.
29. L. P. D'Souza, S. Shree and G. R. Balakrishna, *Industrial & Engineering Chemistry Research*, 2013, **52**, 16162-16168.
30. R. Shwetharani, M. S. Jyothi, P. D. Laveena and R. Geetha Balakrishna, *Photochemistry and photobiology*, 2014, **90**, 1099-1107.

31. B. S. Necula, L. E. Fratila-Apachitei, S. A. Zaat, I. Apachitei and J. Duszczyk, *Acta biomaterialia*, 2009, **5**, 3573-3580.
32. T. I. T. Saito, J. Horie and T. Morioka, *J Photochem. Photobiol. B: Biol.*, 1992, **14**, 369-379.
33. C. Venkobachar, Leela Iyengar and A. V. S. Prabhakara Rao, *Water research*, 1975, **9**, 119-124.
34. Z. Li, F. Wang, A. Kvit and X. Wang, *The Journal of Physical Chemistry C*, 2015, **119**, 4397-4405.
35. S. Hoang, S. P. Berglund, N. T. Hahn, A. J. Bard and C. B. Mullins, *Journal of the American Chemical Society*, 2012, **134**, 3659-3662.
36. K. Zhao, Z. Wu, R. Tang and Y. Jiang, *Journal of the Korean Chemical Society*, 2013, **57**, 489-492.
37. J. M. Wu and M. L. Tang, *Nanoscale*, 2011, **3**, 3915-3922.
38. J.E. P. Kyung-Hwan Cho, Tetsuya Osaka, Soo-Gil Park, *Electrochimica Acta* 2005, **51**, 956-960.
39. P. K. John C. Ireland, Eugene W. Rice, And Robert M. Clark, *Applied And Environmental Microbiology*, , 1993, **59**, 1668-1670.
40. Y.P. S. Ai-Ping Zhang, *World J Gastroenterol* 2004, **10(21)**, 3191-3193.
41. J. Baudart and P. Lebaron, *J Appl Microbiol*, 2010, **109**, 1253-1264.
42. S. Tavernier and T. Coenye, *PeerJ*, 2015, **3**, e787.
43. S. S. Pin-Ching Maness, Daniel M. Blake, Zheng Huang, And A. W. A. J. Edward J. Wolfrum, *Applied And Environmental Microbiology*, 1999, **65**, 4094-4098.

44. R. Shwetharani and R. Geetha Balakrishna, *Journal of Photochemistry and Photobiology A: Chemistry*, 2014, **295**, 11-16.
45. C. D. Jaeger and A. J. Bard, *The Journal of Physical Chemistry*, 1979, **83**, 3146-3152.
46. W. W. D. Ikulchiro Iruml, Keith O. Willbourn, Fu-Ren F. Fan, and Allen J. Bard, *The Journal of Physical Chemistry*, 1980, **84**, 3207-3210.
47. R. Geetha Balakrishna and K. G. Lakshminarayana Bhatta, *Environmental Studies*, S. M. Publications, 2013.

Figure captions:

Figure 1. XRD pattern of nano TiO₂ and NFTiO₂

Figure 2. UV-Vis spectra of TiO₂ and NFTiO₂

Figure 3. X-ray photoelectron spectra of NFTiO₂ (a) Wide spectra (b) Ti 2p core level (c) O 1s core level (d) N 1s core level (e) F 1s core level

Figure 4. (a) SEM image of nano titanium dioxide particle (b) EDS image of nano titanium dioxide

Figure 5. (a) SEM image of N-F doped nano titanium dioxide (b) EDS image of NF doped nano titanium dioxide

Figure 6. Photoluminescence spectra of TiO₂ and NFTiO₂ photocatalyst

Figure 7. Presence of bacteria in field water (a) *Bacillus cereus* in field water confirmed by Bacillus cereus agar plate. (b) *Salmonella and shigella sp.*, confirmed by SS agar plate. (c) *Escherichia coli* is confirmed by EMB agar; Levine plate. (d) *Pseudomonas sp* is confirmed by Pseudomonas fluorescein agar plate. (e) *Staphylococcus aureus* is confirmed by Mannitol salt agar plate.

Figure 8. Effect of photocatalyst on survival fraction of bacteria

Figure 9. Extent of MDA release on photocatalyst treatment

Figure 10. Extent of DNA release on photocatalyst treatment

Figure 11. Extent of RNA release on photocatalyst treatment

Figure 12. Extent of protein release on photocatalyst treatment

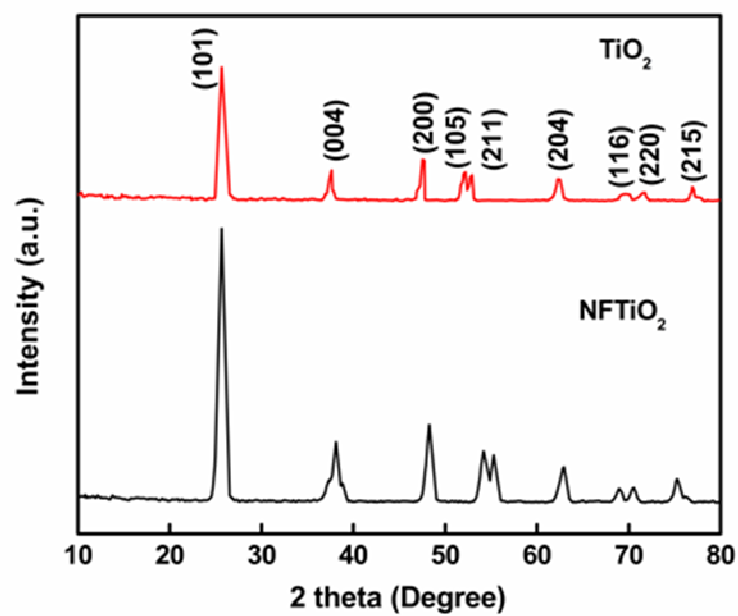


Figure 1. XRD pattern of nano TiO_2 and NFTiO_2

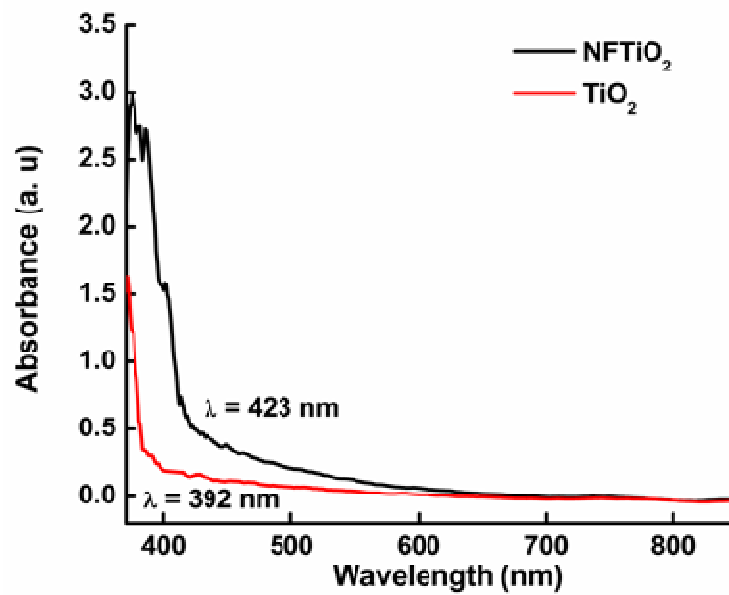


Figure 2. UV-Vis spectra of TiO₂ and NFTiO₂

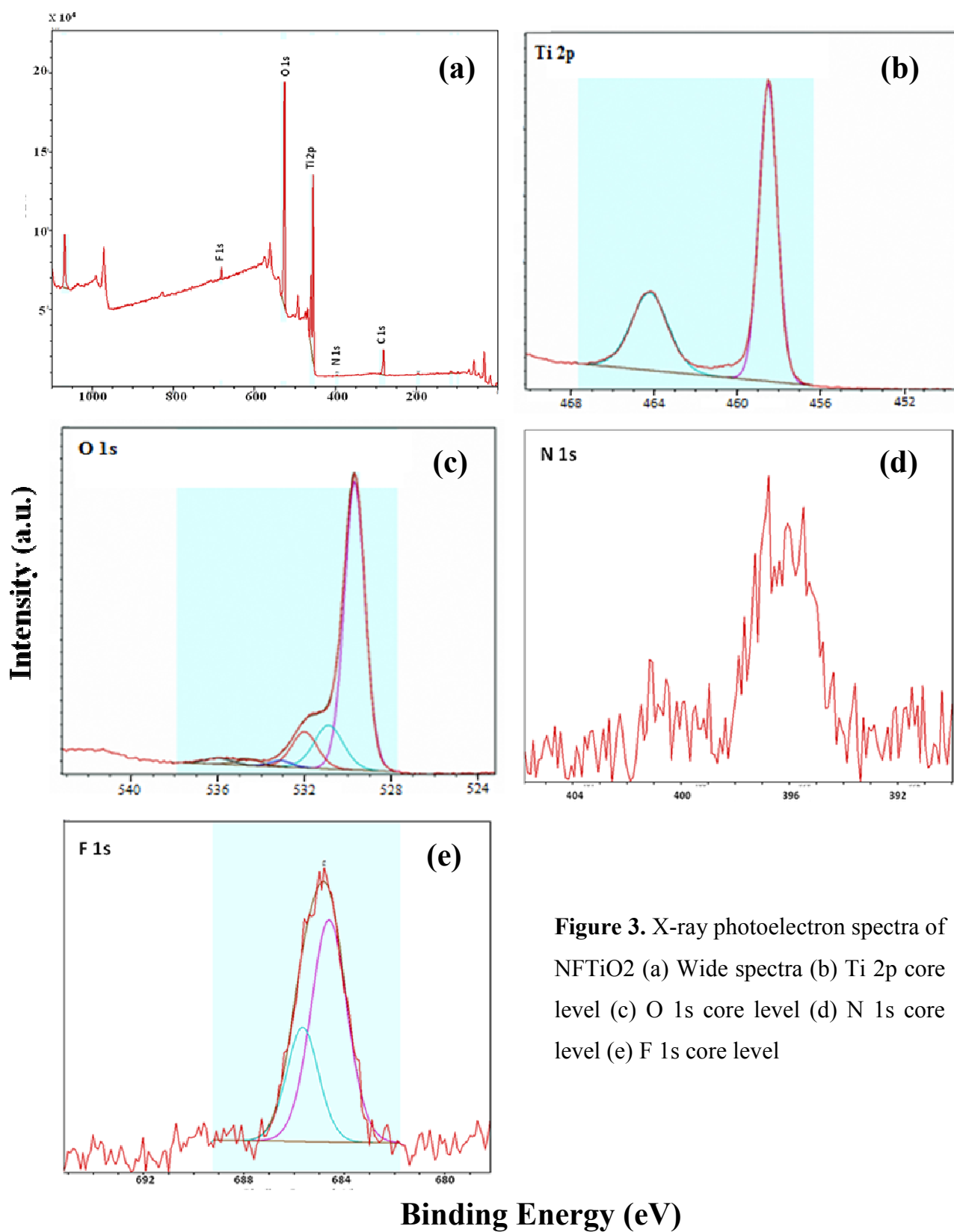


Figure 3. X-ray photoelectron spectra of NFTiO₂ (a) Wide spectra (b) Ti 2p core level (c) O 1s core level (d) N 1s core level (e) F 1s core level

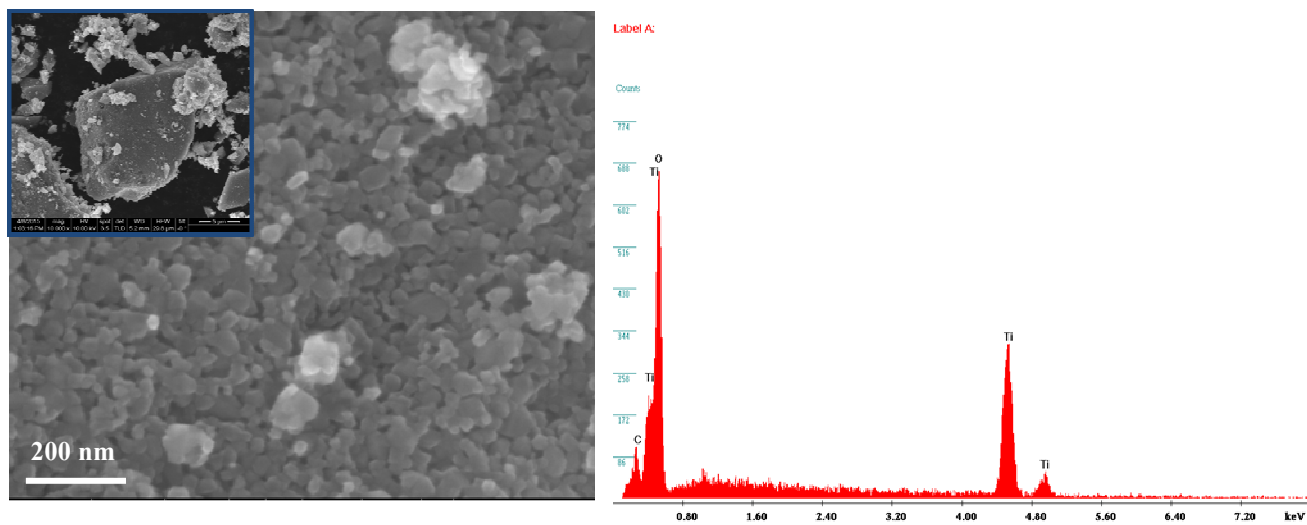


Figure 4. (a) SEM image of nano titanium dioxide particle (b) EDS image of nano titanium dioxide

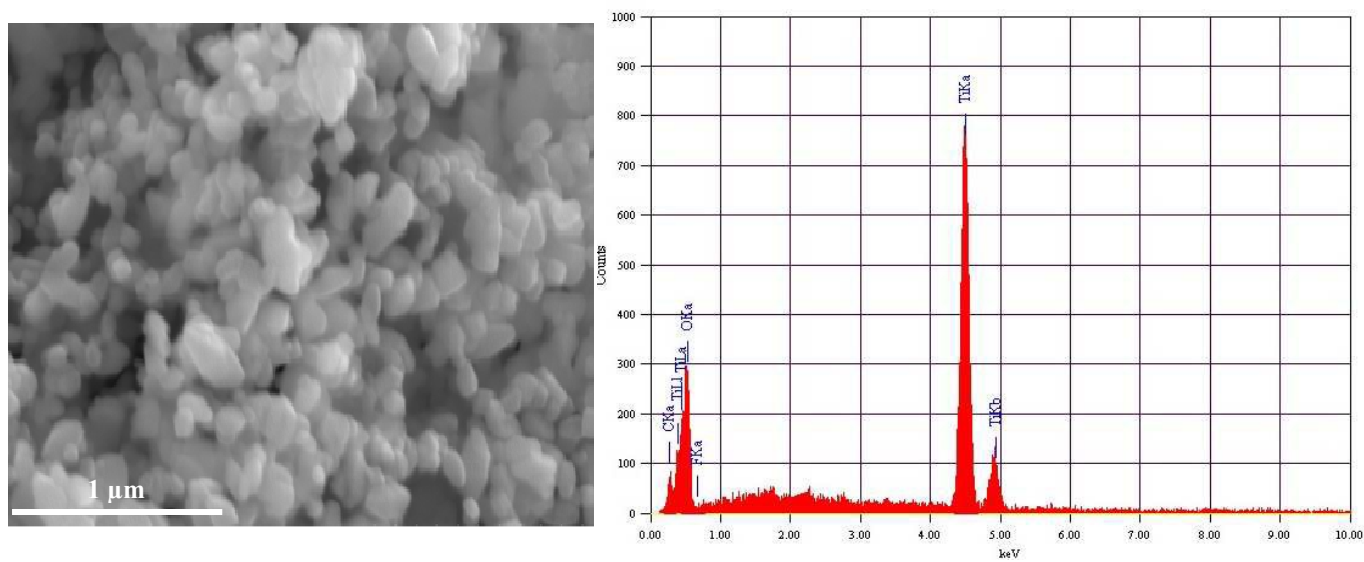


Figure 5. (a) SEM image of NF doped nano titanium dioxide (b) EDS image of NF doped nano titanium dioxide

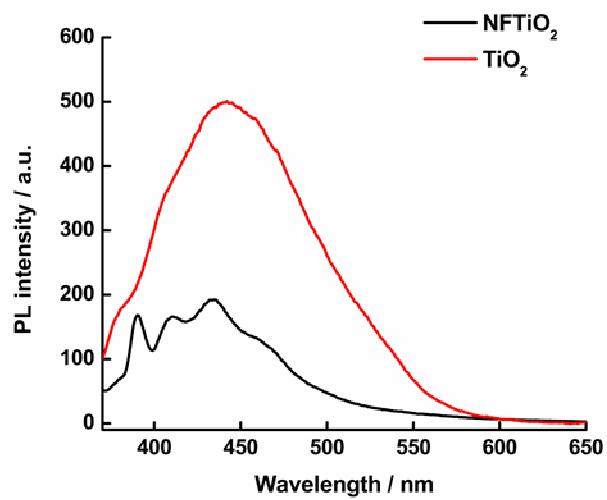


Figure 6. Photoluminescence spectra of TiO_2 and NFTiO_2 photocatalyst

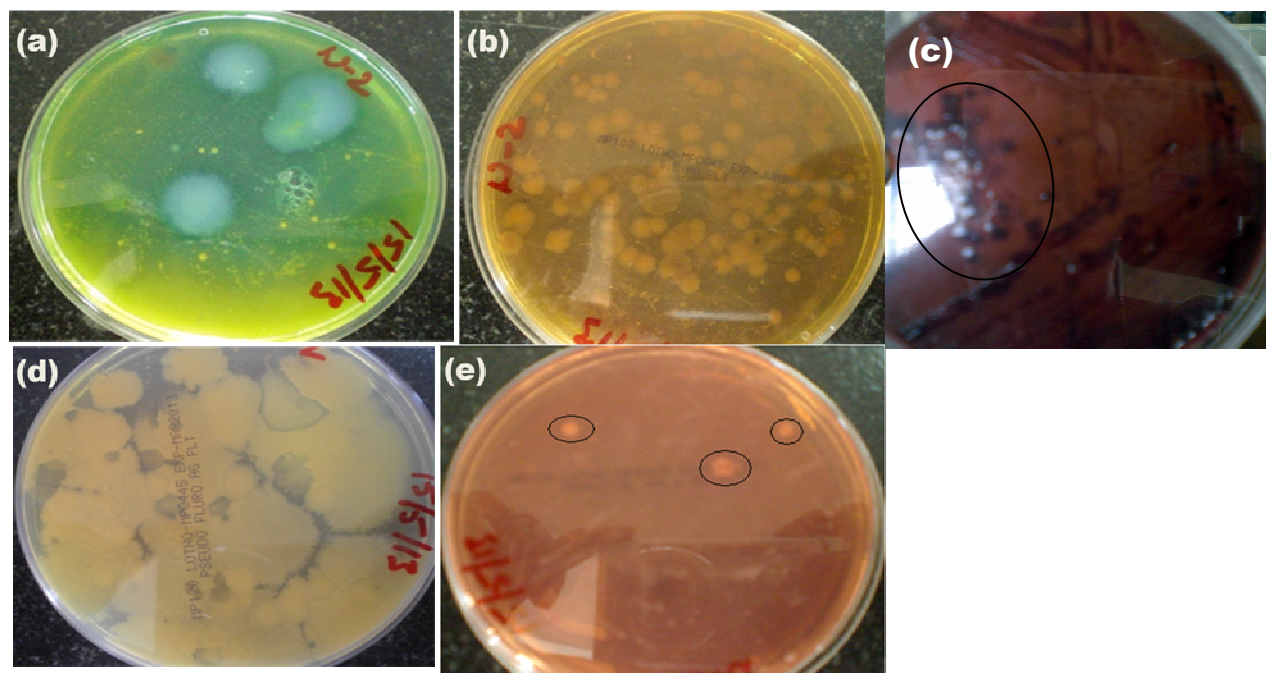


Figure 7. Presence of bacteria in field water (a) *Bacillus cereus* in field water confirmed by *Bacillus cereus* agar plate. (b) *Salmonella and shigella sp.*, confirmed by SS agar plate. (c) *Escherichia coli* is confirmed by EMB agar; Levine plate. (d) *Pseudomonas sp* is confirmed by *Pseudomonas fluorescein* agar plate. (e) *Staphylococcus aureus* is confirmed by Mannitol salt agar plate.

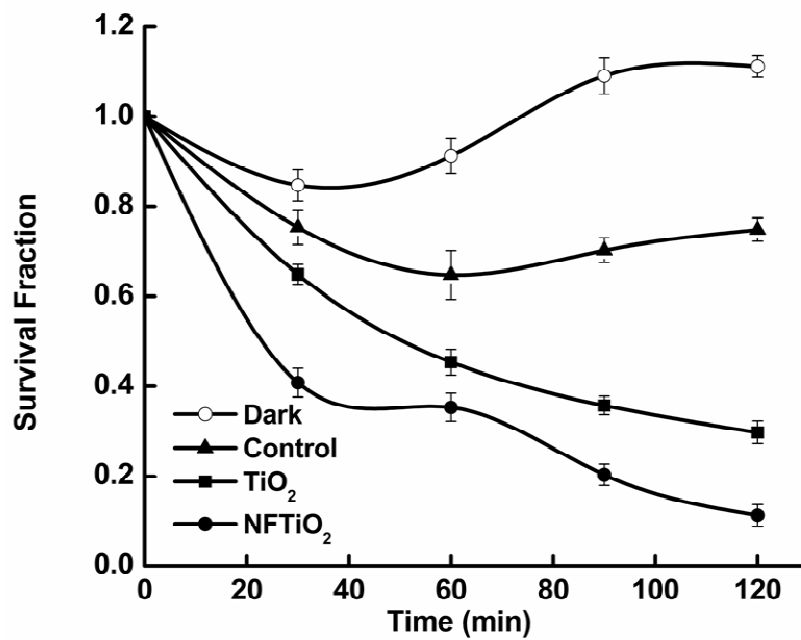


Figure 8. Effect of photocatalyst on survival fraction of bacteria

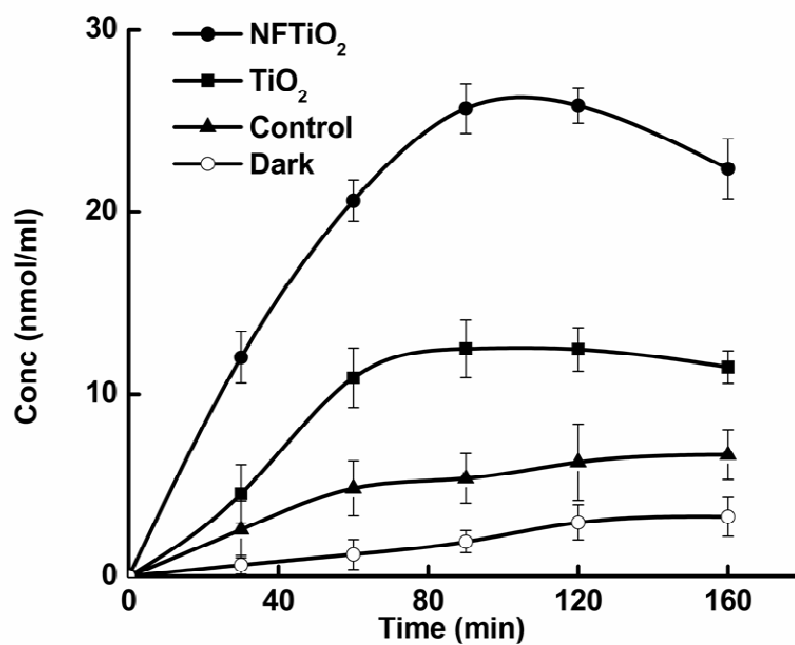


Figure 9. Extent of MDA release on photocatalyst treatment

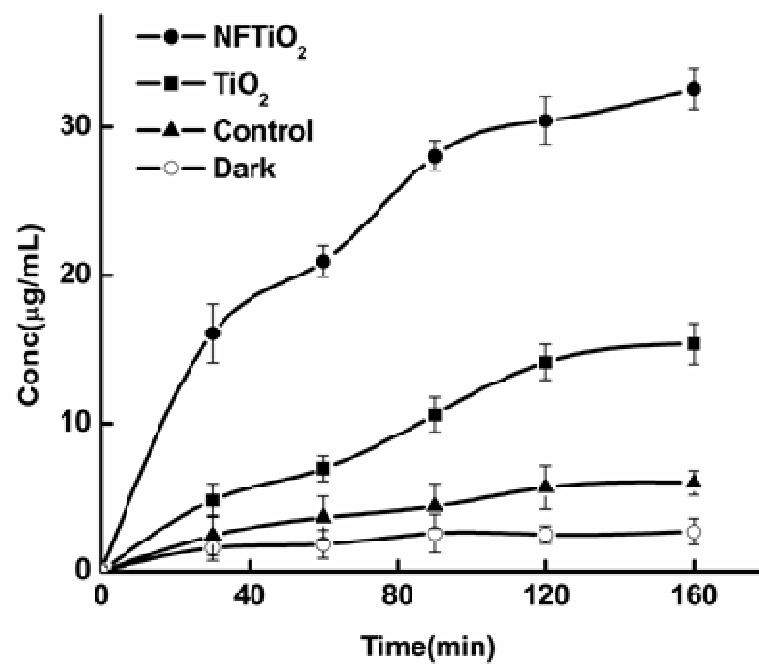


Figure 10. Extent of DNA release on photocatalyst treatment

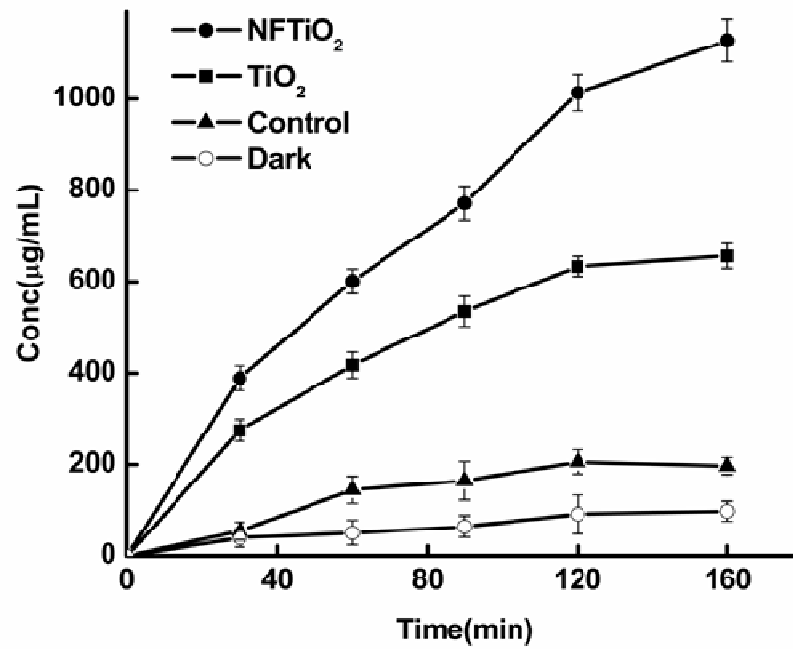


Figure 11. Extent of RNA release on photocatalyst treatment

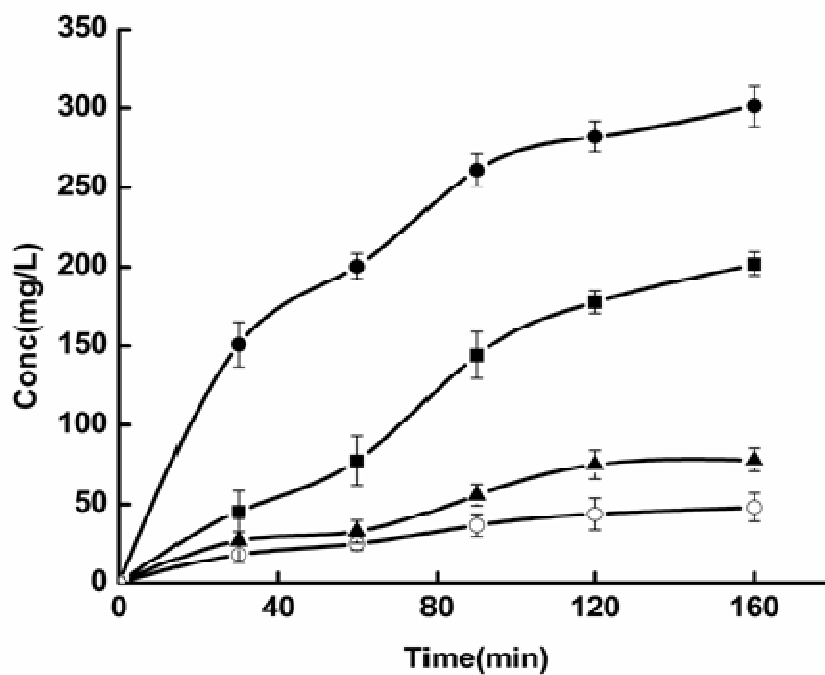
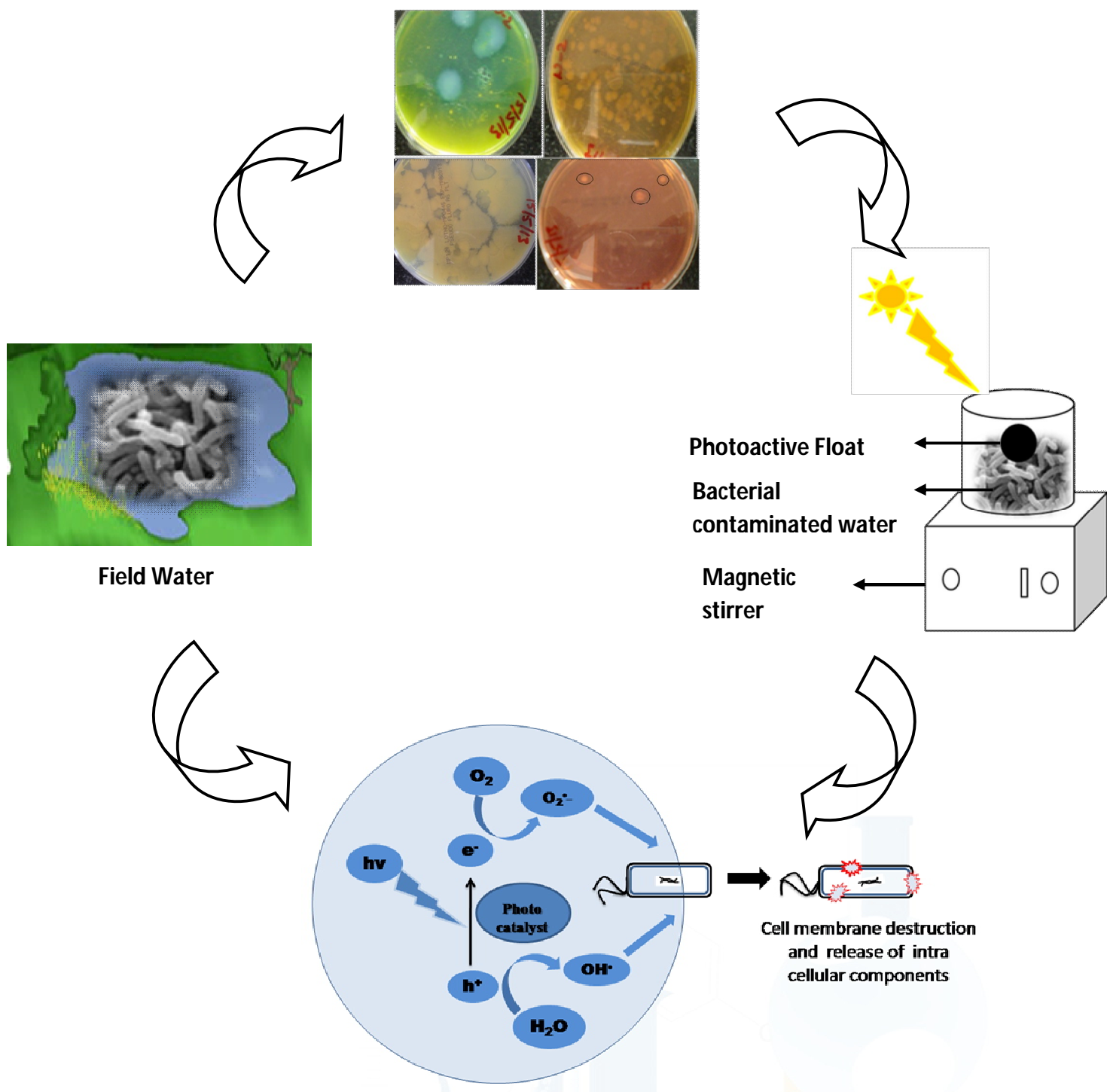


Figure 12. Extent of protein release on photocatalyst treatment

Graphical Abstract

Disinfection of field water contaminated with wide array of bacteria (gram negative and gram positive) using reusable photoactive float fabricated with visible light active nanostructured $NFTiO_2$